The Effect of Interfacial Reaction Layer Thickness on Fracture of Titanium-SiC Particulate Composites

A.J. REEVES, H. DUNLOP, and T.W. CLYNE

Composites of commercial-purity Ti reinforced with 10 vol pct of SiC particles have been produced by cospraying and by powder blending and extrusion. Interfacial reaction layers have been studied by electron and optical microscopy and by Auger electron spectroscopy (AES) of fracture surfaces. The work of fracture has been measured as a function of reaction layer thickness for extruded and heat-treated composites. Material with very thin reaction layers ($<\sim 0.1$ μm) can be produced by cospraying, but porosity levels are relatively high (~ 5 to 10 pct). Extruded material has been produced with a thin reaction layer (~ 0.2 μm) and low porosity (<1 pct). It appears that the rate of reaction conforms with published parabolic rate constant data over a wide range of time and temperature. The reaction layer always consists of TiC and Ti_5Si_3, but the TiC grains tend to be larger than those of Ti_5Si_3. As the reaction layer thickness becomes greater than about 1 μm, the work of fracture falls sharply and the cracking pattern changes from one involving fracture of SiC particles to one in which cracking between the particles and adjacent reaction zones becomes predominant. It is suggested that the volume contraction accompanying this reaction, calculated at about 4.6 pct from density data, has a significant effect in promoting crack formation in these locations by generating radial tensile stresses across the interface. Thus, for this particular composite system, the important effect of a thicker reaction layer may be that it promotes the formation of an interfacial crack *via* an effect on the local stress state, rather than itself constituting a larger flaw in the form of a through-thickness crack assumed to be present.

I. INTRODUCTION

THERE is interest in the reinforcement of titanium with particulate ceramic. This offers the advantage of easier processing compared with fibers, albeit with reduced scope for enhancement of stiffness and creep resistance. However, there is concern about the difficulty of avoiding a degree of interfacial chemical reaction during fabrication or in service. The most popular reinforcement has been SiC. In this case, the reaction, involving formation of TiC and Ti_5Si_3, has been extensively studied.[1-5] Some attention has been devoted to countermeasures, such as barrier layers[6-9] on fibers, but there are difficulties in producing these on particles.

There is some published information concerning the effect of this interfacial reaction on the mechanical behavior of Ti-SiC composites. Early correlations[10] were established for long fiber composites between thickening of the reaction zone and degradation of strength, particularly when the thickness of the layer is greater than about 1 μm. This is often attributed to a weakening of the fiber as a result of the tendency for cracks to propagate in from the reaction layer. Consistent with this is the improved performance obtained with commercial SiC fibers having thick outer layers of pyrocarbon which are relatively compliant and tough. This improvement tends to persist until the pyrocarbon layer is consumed; while a significant proportion of the layer may react during processing, it should then survive for prolonged periods during elevated temperature service.

The details of the reaction can be complex, apparently involving transient formation of a ternary Ti-Si-C phase with a very similar structure to Ti_5Si_3,[11] at least with fibers having carbon-rich surface layers. For lightly reacted specimens, fracture tends to occur between the pyrocarbon layer and TiC reaction product, but after further reaction, failure is often initiated at the interface with the underlying SiC fiber.[12] A further point to note about Ti reinforced with long fibers concerns the danger of oxygen passing rapidly along the interface (from a free surface), consuming any carbon-rich layer and quickly forming a thick oxide layer. This has been noted with both Ti-6Al-4V (α/β)[12,13] and Ti-15V-3Al-3Cr-3Sn (fully β)[14] matrices, accentuating interfacial failure and crack initiation in both cases. Although there is some evidence for differential reaction rates for α and β phases,[3] it appears that attack takes place with both types of matrix phase and that the rate is not highly sensitive to solute content.

There is less information available for particulate Ti composites, in which there would not normally be any interfacial coating as such—except possibly an oxide generated by prior heating of the reinforcement. Loretto and Konitzer[15] have studied fracture paths in composites of Ti-6Al-4V containing SiC or TiC particles, made by powder blending and hot pressing (involving an unspecified thermal history). A thick ($> \sim 1$ μm) reaction zone was present for the SiC case but not with the TiC particles. Loretto and Konitzer observed that cracking occurred between the SiC and the reaction product mixture, but that the TiC particles (which were porous) fractured internally, with the interface remaining intact. They

A.J. REEVES, Research Student, and T.W. CLYNE, Lecturer, are with the Department of Materials Science, Cambridge University, Cambridge CB2 3QZ, United Kingdom. H. DUNLOP, Research Scientist, is with the Pechiney Research Centre, Voreppe, Genoble, France.

Manuscript submitted March 21, 1991.

also reported brittle failure of the matrix in the SiC composite, which was attributed to dissolution in the Ti of carbon released from the SiC. Very low ductility, and hence a low tensile strength, resulted from this, but at elevated temperature the effect was reduced and the SiC composite strength exceeded those of both matrix and TiC composite. Other reinforcements, such as B_4C,[16] have also been investigated, but few data are available on the mechanical properties of such systems.

In the present work, composites of commercial-purity titanium reinforced with SiC particles have been produced with a range of interfacial reaction zone thicknesses. These have been deformed and fractured, and observations have been made on how the nature of the interface appears to affect crack propagation. The objective of this work is to clarify the degree to which progressive reaction must be controlled in this system if a useful combination of properties is to be retained and to examine the scope for achieving this with available fabrication procedures.

II. EXPERIMENTAL PROCEDURE

A. *Composite Production*

Composites were produced from Ti and SiC powders by (a) cospraying and (b) dry blending followed by hot extrusion. The commercial-purity Ti powder, supplied by Alloy Metals Inc., Troy, MI, under the tradename "Amdry," was in the approximate size range of 30 to 150 μm. Only the finer fraction (<75 μm) was used for cospraying. The oxygen level in this material is rather variable, with values up to about 1.5 wt pct being recorded; however, some of this is apparently[16] in the form of Ca-rich oxide particles present as impurities, and the level of oxygen in solution in the titanium is thought to be considerably lower. The SiC particulate used was commercial polishing-grade material in the size range of 15 to 30 μm.

Spray deposition was carried out using the vacuum plasma spray (VPS) process[17–20] under the conditions shown in Table I. In view of the tendency for titanium droplets to absorb hydrogen and nitrogen during passage through the torch, these gases could not be used in the plasma; an argon-helium mixture was employed, with the lower rate of enthalpy release for these gases being compensated by a high plasma current to ensure an adequate energy density to melt the titanium. The SiC particles did not reach their sublimation temperature (~2700 °C) during the process and remained solid throughout, their incorporation into the deposit being largely due to their becoming embedded on impact,[16] with in-flight collisions relatively rare. Relative feed rates of the two powders were adjusted to give approximately 10 vol pct of SiC in the deposit. The Ti powder was, in all cases, injected at the throat of the torch nozzle, with the SiC particles being introduced either into the same region ("coinjected") or at a point about 100 mm from the throat ("downstream injected").

Table I. Conditions for Cospraying of Ti and SiC Powders

Plasma current	950 A
Voltage	40 V
Input power	38 kW
Plasma jet power*	19 kW
Nozzle bore diameter	6 mm
Substrate standoff distance	300 mm
Chamber pressure	200 mbar
Plasma Gas Flow Rates	
Ar	30 L/min
He	40 L/min

*Calculated from the measured power loss to the gun cooling system.

The powder-blended composites were made by dry mixing (of proportions corresponding to 10 vol pct SiC) in a ball mill, followed by cold pressing into a copper can. This was then evacuated, heated, and sealed by electron beam welding. The can was held for 2 hours in a furnace at 900 °C and then extruded in a circular section die of diameter 20 mm, with a die semiangle of 45 deg and an extrusion ratio of about 17. The extrusion chamber was held at about 450 °C and the die at about 250 °C. As a result of the low thermal diffusivity of the powder compact, different regions of the composite experienced rather different thermal histories during heating prior to extrusion, but there was, in any event, very incomplete Ti-SiC interfacial contact during this period. Effective exposure of the consolidated interface to temperatures of around 900 °C was limited to a period of a few minutes during extrusion. Some specimens were subsequently heat-treated in argon-filled sealed ampoules at 950 °C for different periods, in order to build up reaction layers of variable thickness.

B. *Microstructural Examination*

Metallographic polished sections of the as-sprayed and heat-treated specimens were prepared using various grades of diamond polishing media. These specimens were examined optically and with a scanning electron microscope (SEM) using secondary and backscattered imaging modes. Polished sections were also produced from fractured specimens subjected to impact testing (Section D). These were cut normal to the fracture surface, with the edge protected by nickel coating prior to mounting and polishing. For transmission electron microscope (TEM) specimens, 3-mm discs were ground, dimpled, and ion-milled to perforation in a conventional manner. Examination was carried out using PHILIPS* 400T and JEOL 120CX microscopes.

*PHILIPS is a trademark of Philips Electronic Instruments Corporation, Mahwah, NJ.

Porosity measurements were made by Archimedean picnometry, using a high precision (±10 μg) balance. Pore content evaluation could not be done very accurately for the sprayed material because of the uncertainty concerning the exact volume fraction of SiC: this was evaluated metallographically, but the operation is rather imprecise in view of the danger of matrix smearing or particle excavation during polishing. The porosity level of as-sprayed material was found to be about 3 to 10 pct, while the powder-blended composites had pore contents of around 0.5 pct in the as-extruded condition (Section III–B).

C. *Chemical Analysis of Fracture Surfaces*

Local chemical analysis of fracture surfaces was carried out by high-resolution scanning Auger microscopy in the Cameca Nanoscan 50 installed at the Pechiney Research Centre in Voreppe, France. The field emission gun of this system has the advantage of providing a small spot size with high brightness at low primary beam energies. Auger spectra were acquired at an accelerating voltage of 8 kV, with a beam current of 3 to 4 nA (survey scans) and ~25 nA (high-resolution scans). The primary beam diameter under these conditions was approximately 50 to 70 nm. All spectra were obtained by direct $N(E)$ pulse counting, at constant energy resolution ΔE.

In order to avoid surface contamination by adventitious carbon and oxygen, specimens were fractured *in situ* under ultra high vacuum (UHV) ($<10^{-9}$ torr). The freshly created fracture surfaces were rapidly examined by SEM using secondary electrons before selection of regions of interest for Auger microanalysis. Zones analyzed covered a diameter of 100 to 200 nm and a depth of 1 to 8 nm. A vacuum of better than 4×10^{-10} was maintained during all of the analyses.

D. *Mechanical Testing*

In this study, the mechanical testing was limited to some measurements of the work of fracture, using a "Frank" impact testing machine, similar to a standard Izod configuration. This involved striking an unnotched cylindrical bar with a pendulum to generate three-point bending in the specimen. The absorbed energy was divided by the nominal cross-sectional area to give the work of fracture. Specimen diameters were all about 3 mm. In most cases, three specimens of each type were tested. The significance of a work of fracture measurement obtained in this way for particulate metal matrix composites (MMCs) is discussed by Daimaru *et al.*,[21] who conclude that the parameter should give a reliable indication of the toughness of the material.

III. RESULTS AND DISCUSSION

A. *Progression of the Interfacial Reaction*

Examination of the cosprayed material allowed the early stages of the reaction to be studied, because in these specimens, the interface had only been subjected to a very short period at elevated temperature. The TEM micrographs of interfacial regions shown in Figure 1 illustrate this point. In Figure 1(a), which is from a downstream-injected composite, no obvious reaction layer is apparent, although some bright regions can be seen which probably represent areas of interfacial decohesion. Even if these are reaction layers, they do not cover the interface and they are no more than about 10 nm in thickness. The interface in the coinjected specimen shown in Figure 1(b), however, exhibits a well-defined reaction layer about 50 to 100 nm in thickness. This may be compared with the interfacial structure of the powder-blended and extruded specimen shown in Figure 1(c), in which the layer thickness is about 0.1 to 0.2 μm, which is rather similar to that in the cosprayed material. The effect of heat-treating the extruded material can be seen in

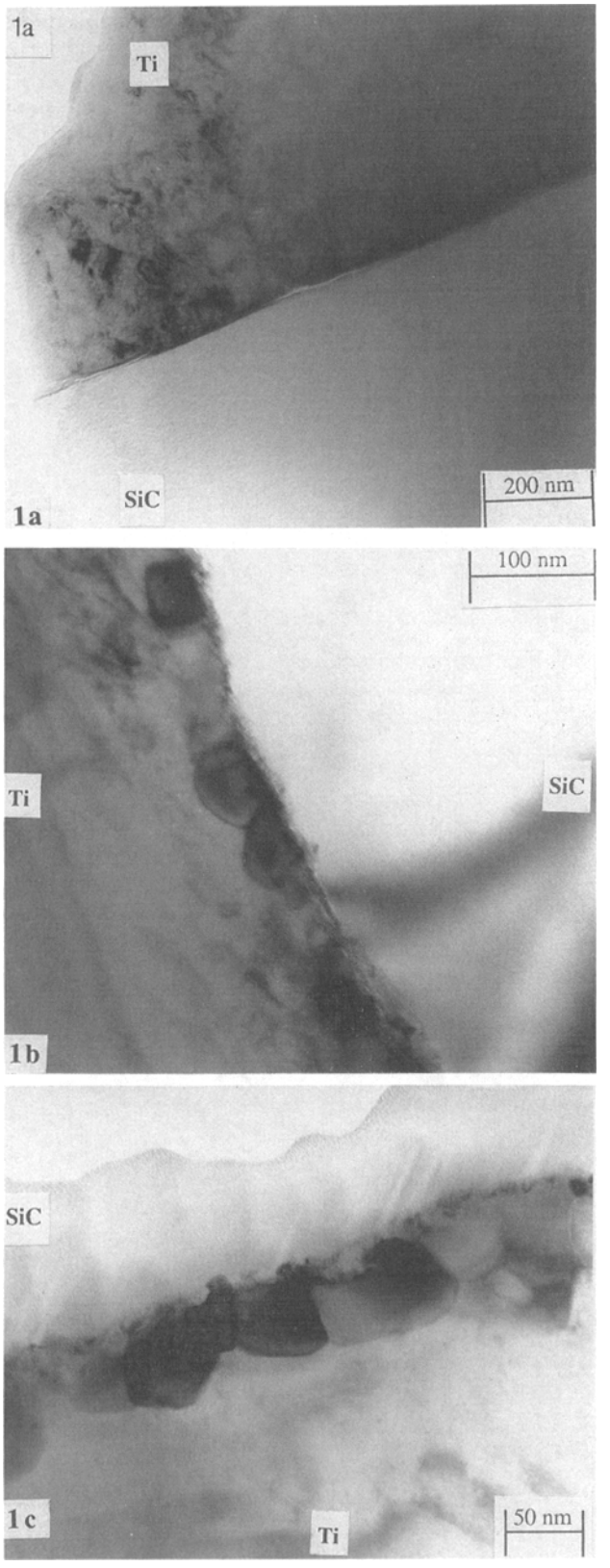

Fig. 1—TEM bright-field images showing typical interfacial regions in specimens produced by (*a*) cospraying with downstream injection of the SiC, (*b*) cospraying with powders injected in the same region, and (*c*) as-extruded after powder blending.

Figure 2, which shows optical micrographs of specimens in (a) the as-extruded state and after (b) 40 minutes and (c) 300 minutes at 950 °C. A progressive increase in the layer thickness is evident here, from submicron (not visible) to several microns.

Reaction layer thickness data taken from such microstructural observations are presented in Figure 3. This

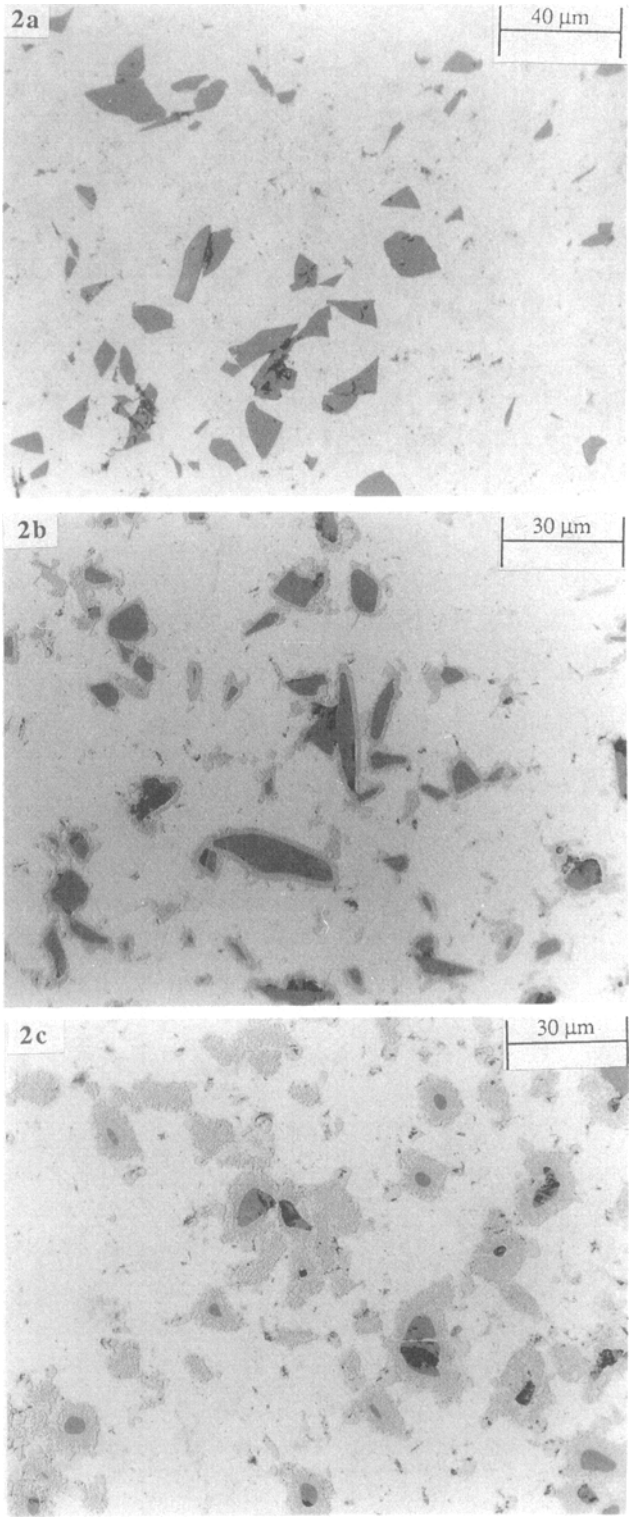

Fig. 2—Optical micrographs of extruded composites (*a*) as-extruded, (*b*) after 40 min at 950 °C, and (*c*) after 300 min at 950 °C.

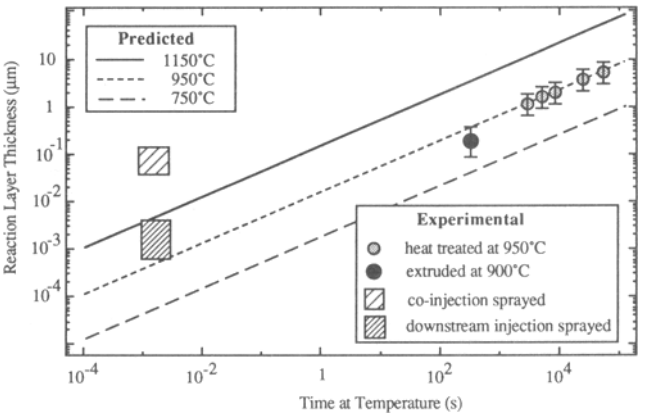

Fig. 3—Plot of reaction layer thickness as a function of time at temperature, comparing experimental data for extruded and sprayed composites with predictions obtained for three temperatures using parabolic rate constants established by Martineau *et al.*[1]

shows the thickness plotted as a function of time at temperature, together with predictions (for three different temperatures) obtained using parabolic rate constants obtained experimentally by Martineau *et al.*[1] For the heat-treated specimens, it is clearly the annealing treatments which have dictated the layer thickness, and as these are well defined, there is no difficulty in placing the corresponding points on the plot. It can be seen that these points are closely consistent with the rate constants from the previous study,[1] which were obtained in a similar manner on quite heavily reacted material.

It is rather more difficult to place points from the sprayed and as-extruded specimens, in view of uncertainties about the precise thermal histories experienced by the interfaces. In Figure 3, the interface for the as-extruded case is taken as having spent a period of a few minutes (during extrusion) at the billet temperature of about 900 °C. This appears to fit in well with the rest of the data. Placement of data for the sprayed specimens on this plot is more speculative, but it is known[22] that the flight time in VPS is about 1 ms, while the post-impact cooling period down to the temperature of the deposit (<700 °C here and, hence, below the reaction range) would typically be a few milliseconds. Taking in-flight collisions as unlikely in both cases, each interface would therefore have been subject to a few milliseconds at high temperature, followed later by a further similar period when the SiC particle is covered by an arriving Ti droplet. The difference between the two cases arises because the downstream-injected SiC particles did not enter the hottest part of the plasma and so were much cooler on impact. This is broadly consistent with Figure 3, from which effective interfacial temperatures during reaction for downstream and coninjected cases would appear to be of the order of 1000 °C and 1400 °C, respectively. These values are broadly of the order expected, suggesting that the reported rate constants may be applicable from the very early stages of the reaction. This would be consistent with the observation that both Ti_5Si_3 and TiC appear to be formed from the outset (Figure 1(b)).

A further point of note concerning the progression of the reaction is that the TiC phase tends to form as much

larger grains than does the Ti_5Si_3 phase. For example, Figure 4(a) is a TEM micrograph of an interfacial region in a specimen held for 40 minutes at 950 °C, showing a bright-field image of a large TiC particle and the corresponding diffraction pattern from the [001] zone axis. This tendency becomes evident in optical micrographs for heavily reacted specimens; Figure 4(b) shows the microstructure after 660 minutes at 950 °C, in which the TiC particles are apparent as discrete precipitates several microns in diameter. This tendency for growth of TiC, while the Ti_5Si_3 grains remain small, may be associated with the wide stoichiometric range of the phase, which is sometimes designated TiC_{1-x} in view of the scope for carbon depletion.[23] This may allow easy transport of carbon through the phase to allow the reaction to proceed, while the reactants can only migrate past Ti_5Si_3 particles by grain boundary diffusion. The formation of large TiC particles might be expected to cause localization of the transformation strains and, hence, to encourage cracking (Section B).

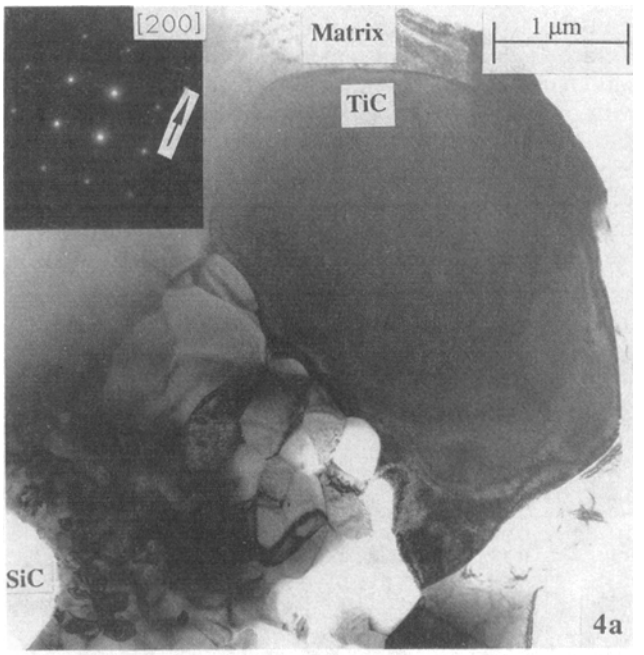

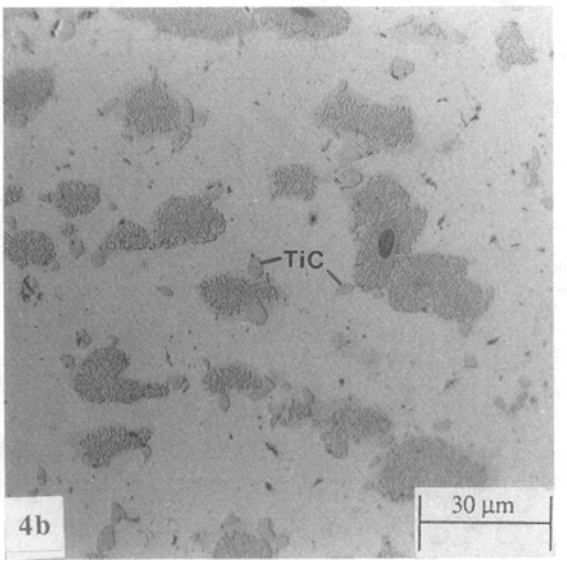

Fig. 4—Micrographs illustrating the tendency for large particles of TiC to form after prolonged heat treatment: (*a*) bright-field TEM micrograph, together with a diffraction pattern obtained from the large TiC particle, of a specimen held for 40 min at 950 °C and (*b*) optical micrograph of a specimen held for 660 min at 950 °C.

Table II. Measured Fracture Energy Values for Extruded and Heat-Treated Specimens, Together with Porosity Values Obtained after Impact Loading for Those Specimens with the Highest and Lowest Fracture Energies in Each Category

Specimen Thermal History	Fracture Energy ($kJ\ m^{-2}$) Individual	Fracture Energy ($kJ\ m^{-2}$) Mean	Apparent Porosity Level (Pct)
As-extruded	285.9	262 ± 30	0.43
	280.2		—
	220.7		0.70
40 min at 950 °C	219.6	220 ± 54	0.71
	187.4		—
	129.0		1.70
100 min at 950 °C	219.6	178 ± 26	0.52
	177.4		—
	146.0		3.37
500 min at 950 °C	98.4	85 ± 15	1.16
	70.5		3.76

B. *Fracture Behavior*

The fracture energy measurements are shown in Table II and displayed graphically in Figure 5, which is a plot of fracture energy as a function of reaction layer thickness. Evidently, the toughness falls with increasing thickness and will tend to be quite low for layers greater than about 1 to 2 μm. This fall in resistance to fracture is accompanied by a distinct change in preferred crack path, which can be seen in Figure 6. This shows sections normal to the fracture surface for (a) as-extruded and (b) 300 minutes at 950 °C composites. While there is apparently a strong interface in the as-extruded case, with particle fracture common, the heat-treated composite is

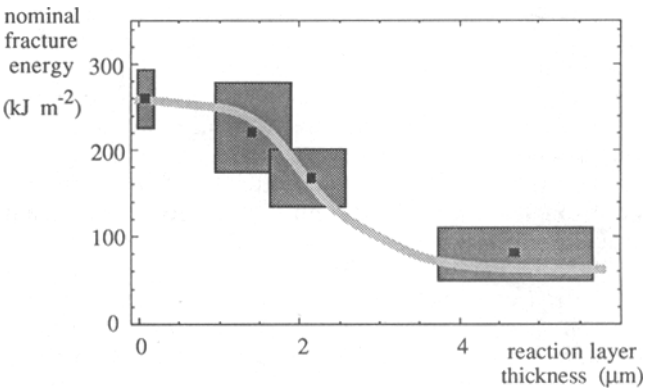

Fig. 5—Fracture energy data shown in Table II, plotted against the thickness of the reaction zone for the specimens concerned.

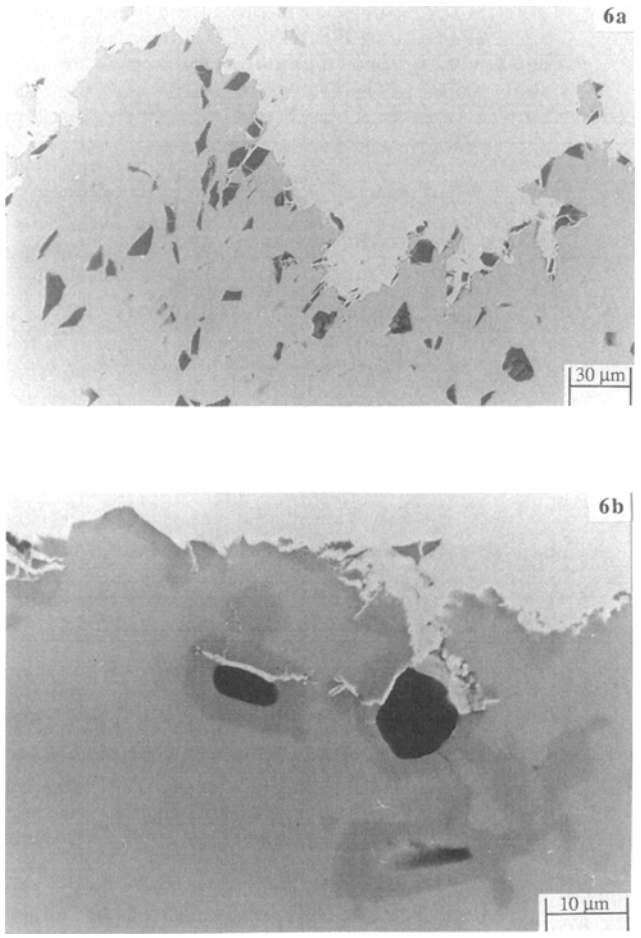

Fig. 6—SEM secondary electron images of polished sections normal to the fracture surface taken from impact loaded specimens (*a*) as-extruded and (*b*) after 300 min at 950 °C.

clearly very prone to crack formation between the SiC particles and their surrounding reaction layers. The appearance of the fracture surfaces in these two cases (Figure 7) suggests that the matrix always fails in an essentially ductile manner, but the ease of interfacial cracking when a significant reaction zone is present clearly embrittles the composite markedly. In Table II, the results of porosity measurements are shown for some of the specimens after impact testing. These are apparent values, based on the assumption that only Ti and SiC (10 vol pct) are present. The increases observed reflect the effect of interfacial cracking promoted by the applied load, rather than being due to porosity arising from the reaction (which should not change the macroscopic volume or mass of the specimen and, hence, would not affect the measurement) or to any differences in the porosity of the original extruded composite. It can be seen that poor toughness correlates with high levels of interfacial cracking.

Surface analysis data from the fracture surface of a cosprayed composite are presented in Figures 8(a) and (b). These show Auger electron spectroscopy (AES) scans obtained with the beam centered on (a) a SiC particle and (b) a region of matrix close to the particle. These locations are marked on the SEM image in Figure 8(a). The particle surface shows no trace of Ti, suggesting either that it has been fractured or that there is poor interfacial adhesion. The latter is the case here, as the particles showed no tendency to break. (The matrix is porous and weak.) Further evidence for this is furnished by the trace of oxygen seen in Figure 8(a), which would not appear on a fractured SiC particle and probably represents an original oxide layer. There may have been insufficient time at high temperature for this to be reduced by the Ti matrix. No trace of Si or C is present in Figure 8(b), giving further confirmation of the lack of any extensive reaction.

Results from the as-extruded specimen are presented in Figure 9, again showing scans from points on and adjacent to a SiC particle. The particle surface (Figure 9(a)) again shows no Ti, but in this case, there is also no oxygen, indicating that it is a fresh cleavage surface. The interfacial region (Figure 9(b)) shows little carbon and only minor superficial silicon. (The Si LVV, with an escape depth $\lambda \sim 1$ nm, is present, but the Si KLL, $\lambda \sim 4$ nm, is absent.) This is in contrast to observations on heat-treated specimens, in which material adjacent to the SiC particles frequently showed strong Si and C peaks. A feature worthy of note in Figure 9(b) is the Cl (LVV) peak. Although the overall chlorine level

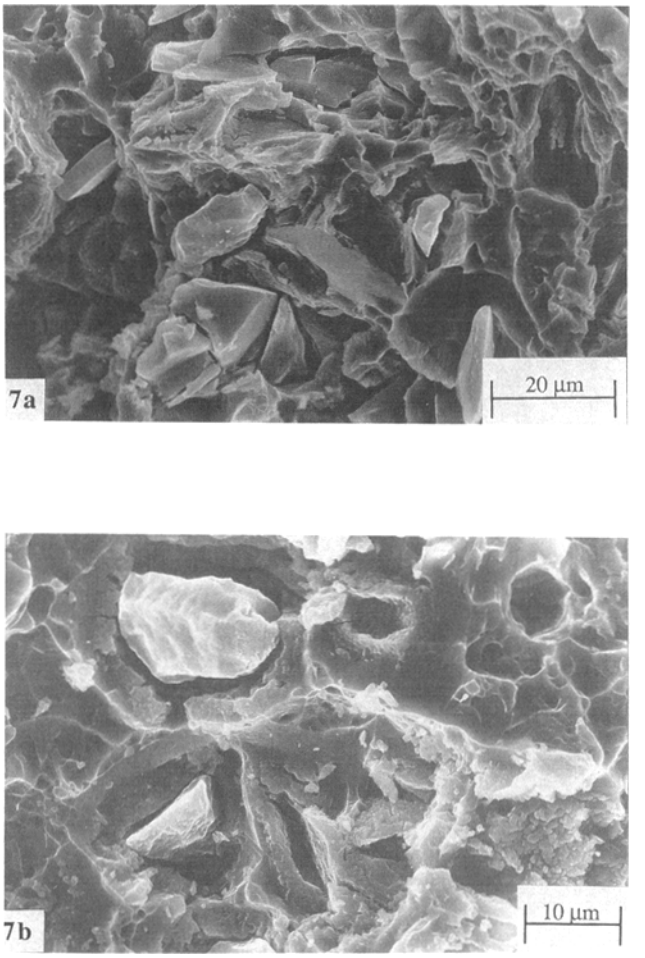

Fig. 7—SEM secondary electron images of fracture surfaces taken from impact-loaded specimens (*a*) as-extruded and (*b*) after 300 min at 950 °C.

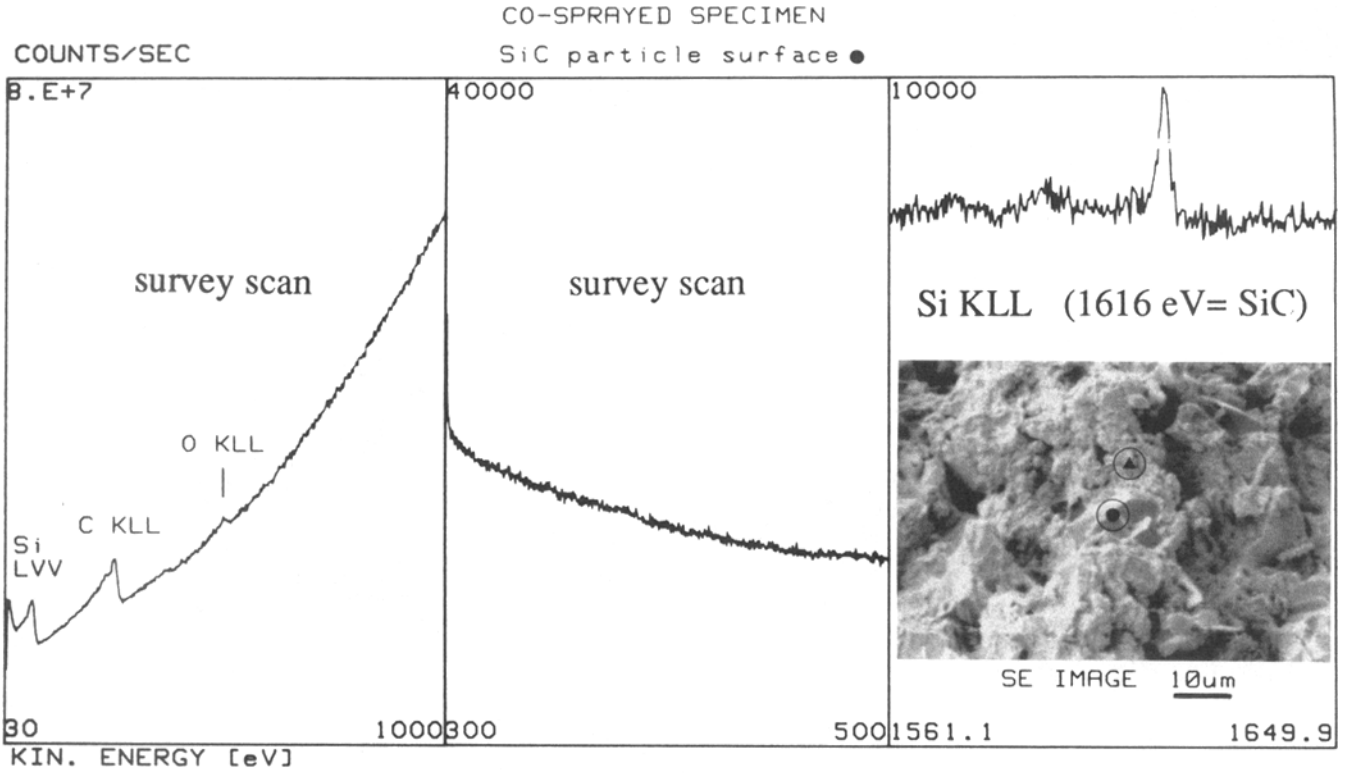

(*a*)

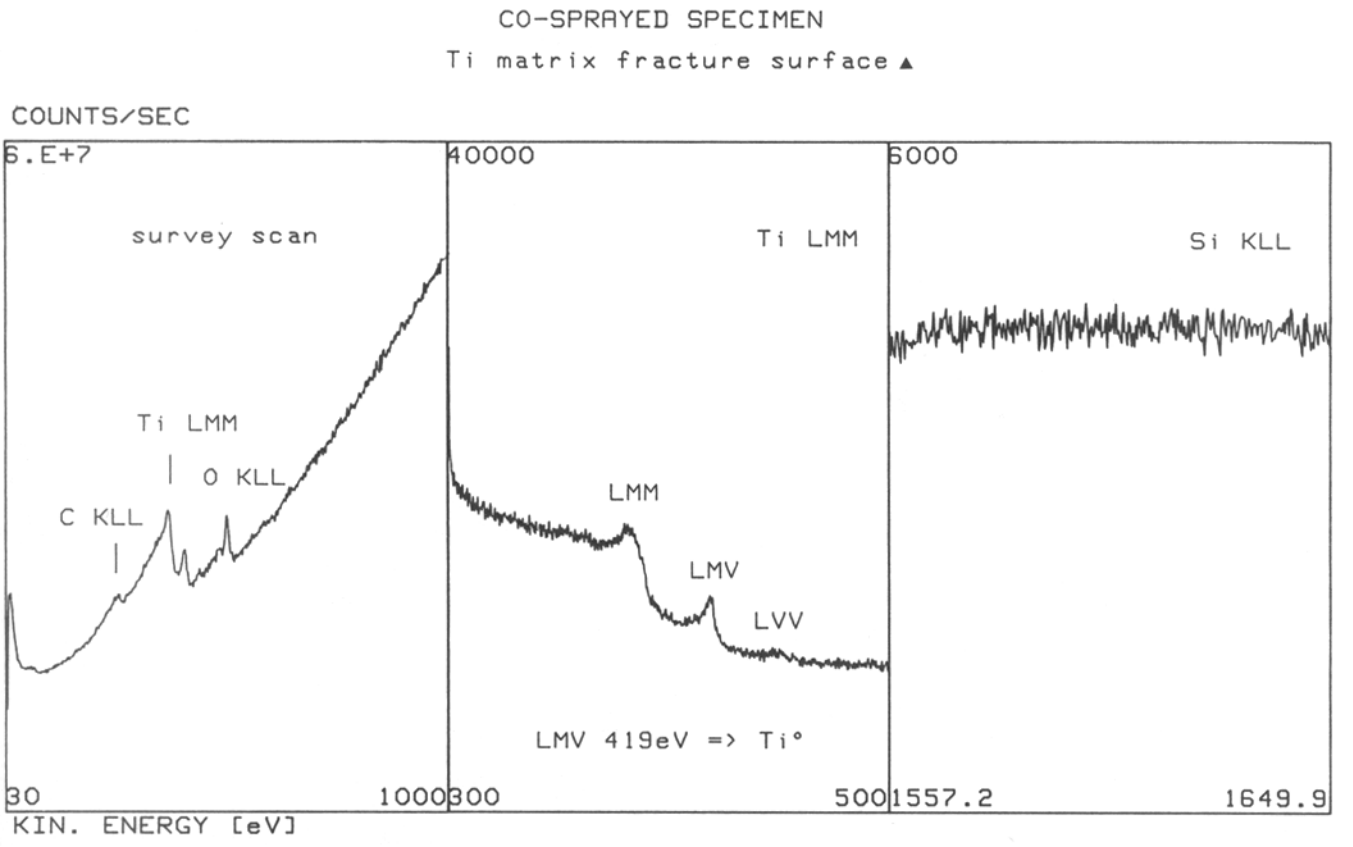

(*b*)

Fig. 8—AES scans from the fracture surface of a coinjected spray-deposited specimen taken from the two points indicated on the inset SEM micrograph: (*a*) is from exposed SiC particle surface and (*b*) is from nearby matrix. Both survey and selected high-resolution scans are shown.

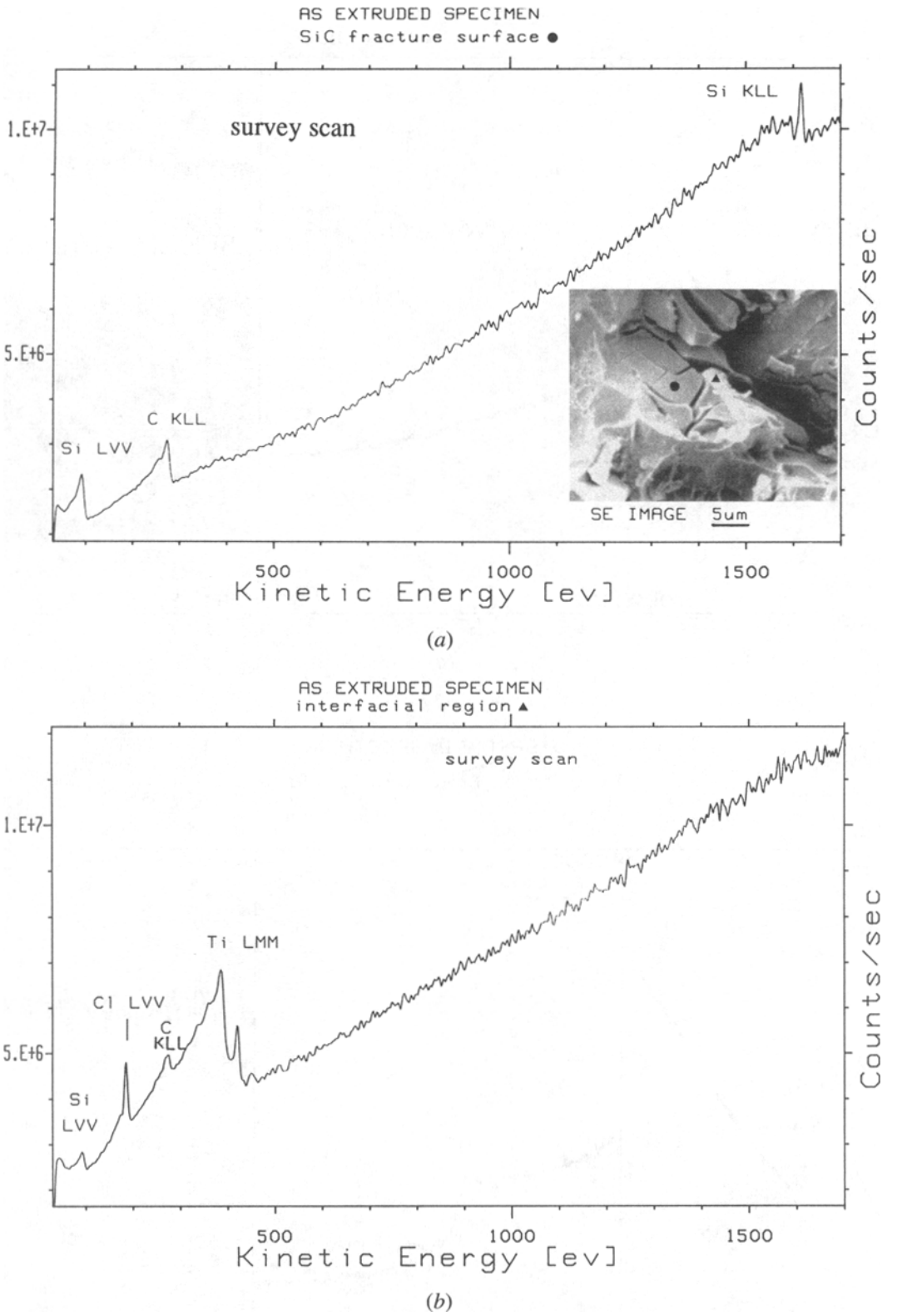

Fig. 9—As for Fig. 8, but with survey scans only, from a powder-blended specimen in the as-extruded state.

(~0.08 wt pct) was not very high, the species is extremely surface active and appeared in several spectra. It can have a marked embrittling effect, although its presence is not thought to be complicating the trends observed in the present work.

The AES scan shown in Figure 10(a) is from an area within a reaction shell, from which a SiC particle has been detached. It exhibits no Si peak but a clear C peak. It seems likely that this is because the beam was centered on a relatively large TiC particle within the reaction zone.

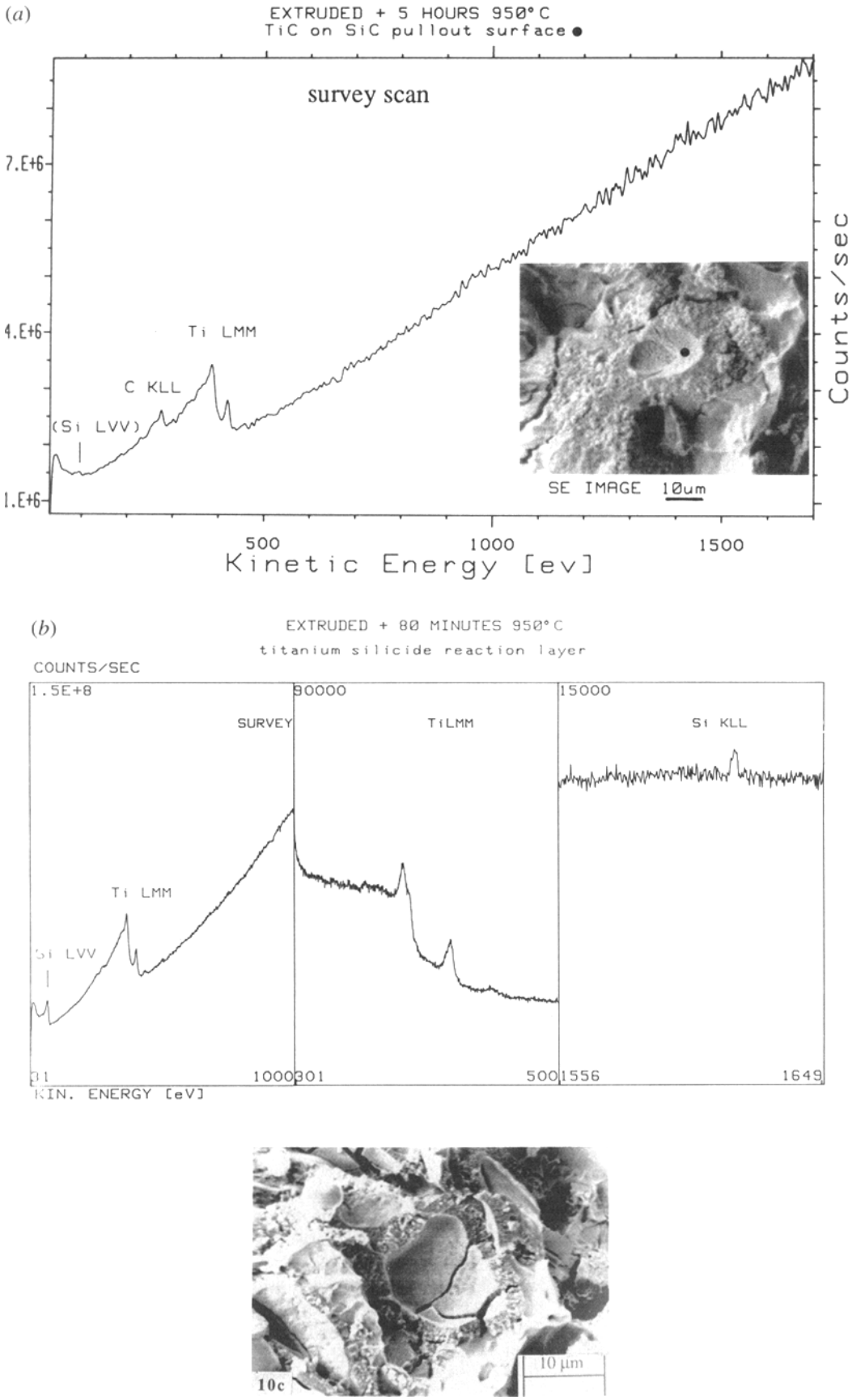

Fig. 10—Data from fracture surfaces of heavily reacted specimens: AES scans, taken from craters which had presumably held SiC particles. (*a*) A survey scan from a specimen subjected to 5 h at 950 °C, apparently with the beam centered on a large TiC particle, (*b*) survey and high-resolution scans from a specimen subjected to 80 min at 950 °C, showing the presence of titanium silicide, and (*c*) SEM micrograph from the specimen of (b), showing extensive cracking of the reaction shell.

However, there is no doubt that the reaction zone also contains titanium silicide, and this was confirmed by spectra such as that shown in Figure 10(b). The reaction shells left by SiC particles are prone to extensive cracking. This can be clearly seen in the SEM micrograph shown in Figure 10(c).

A possible explanation of the tendency for this interfacial reaction to promote cracking so strongly lies in the residual stresses arising from the transformation strain. This is readily estimated from density and molecular weight values for the reactants and products, which are shown in Table III. Also shown in this table are the molar volumes involved in the reaction

$$8Ti + 3SiC \rightarrow 3TiC + Ti_5Si_3 \qquad [1]$$

from which the volume transformation strain Δ_T can be written as

$$\Delta_T = 3\varepsilon_T = \frac{V_{\text{products}} - V_{\text{reactants}}}{V_{\text{reactants}}}$$

$$= \frac{0.11719 - 0.12287}{0.12287} = -4.6 \times 10^{-2} \qquad [2]$$

$$\therefore \varepsilon_T = -1.5 \times 10^{-2} \qquad [3]$$

where ε_T is the linear transformation strain. This volume contraction will tend to set up radial tensile stresses (and hoop stresses which are tensile in the SiC particle and compressive in the matrix) in a similar manner to differential thermal expansion (assuming $\alpha_m > \alpha_p$). In fact, the stresses arising from the transformation strain will tend to offset those already present from differential thermal contraction. That the stresses from this particular reaction can be significant is readily seen by considering an isolated particle and evaluating the radial strain

$$\varepsilon_r = \frac{\varepsilon_T t}{R} \qquad [4]$$

where t is the reaction layer thickness and R is the radius of the particle. If this is set equal to the radial strain from differential thermal contraction during post-fabrication cooling

$$\varepsilon_{\Delta T} = \Delta\alpha\Delta T \qquad [5]$$

Table III. Data[24] Used to Calculate the Volume Change Associated with the Interfacial Reaction*

Phase	Density (kg m^{-3})	Molecular Weight	Reaction Molar Volume (m^3)
Ti (hexagonal)	4510	47.88	0.08493 (8 moles)
SiC (fcc)	3170	40.09	0.03794 (3 moles)
TiC (fcc)	4250	59.89	0.04227 (3 moles)
Ti_5Si_3 (hexagonal)	4320	323.64	0.07492 (1 mole)

*The molar volumes are for the reaction shown as Eq. (1).

an expression is derived for the reaction layer thickness needed to reach this condition

$$t = \frac{R\Delta\alpha\Delta T}{\varepsilon_T} \qquad [6]$$

which, for $R = 10\ \mu$m, $\Delta\alpha = 5 \times 10^{-6}\ K^{-1}$, and $\Delta T = -900$ K, gives a value for t of 3 μm. In fact, there will have been some relaxation of the differential thermal contraction stress during cooling, so that even a thinner reaction layer than this might put the interface into net radial tension.

It would appear likely that such tensile stresses are significant in promoting interfacial cracking and embrittlement of the composite. A schematic illustration of stress distributions around a SiC particle with and without a reaction layer is shown in Figure 11. Although this is a crude picture, neglecting the effects of prior plastic strain and stress relaxation, it illustrates how interfacial cracking will tend to be promoted by the transformation strain. The observed tendency for the cracks to form between the reaction layer and the SiC particle is consistent with this view, as these constituents are both brittle, with less scope for stress relaxation than would be the case at the matrix/reaction layer boundary. The presence of large grains in the reaction layer, reducing the scope for strain accommodation by grain boundary sliding, may also favor cracking, so that the interface between the SiC and adjacent large TiC grains may be a particularly favored crack site. Undoubtedly, the microstructural changes accompanying the reaction also have the effect of reducing the tensile strength of the interface, but it seems likely that these changes in stress state are highly significant; the progressive effect on thickening of the reaction zone would appear to support this view. It is commonly supposed that a reaction layer constitutes a flaw (presumably a through-thickness crack), so that a simple fracture mechanics argument suggests that failure is encouraged by a thicker layer. It seems likely, however, that in the present case, cracks first form parallel to the layer in heavily reacted composites, so that it is not the dimensions of the reaction layer *per se*, but the ease of formation of the crack that is important.

IV. CONCLUSIONS

The following conclusions can be drawn from this work:

1. The kinetics of the reaction conform approximately to the parabolic behavior reported by Martineau *et al.*[1] over a wide range of time and temperature.
2. Cospraying can be used to produce composites with virtually no reaction layer by using a downstream injection technique for the SiC particles. Coinjection gives rise to a reaction layer of the order of 0.1 μm in thickness. As-sprayed material, however, has a relatively high porosity level (~5 to 10 pct). A powder blending and extrusion technique has been used to produce composites with a reaction layer thickness of about 0.2 μm. Heat treatments have been carried out on this material to produce reaction zones several microns in thickness.
3. The reaction layer is made up of Ti_5Si_3 and TiC grains, the latter often becoming much larger in size than the former.

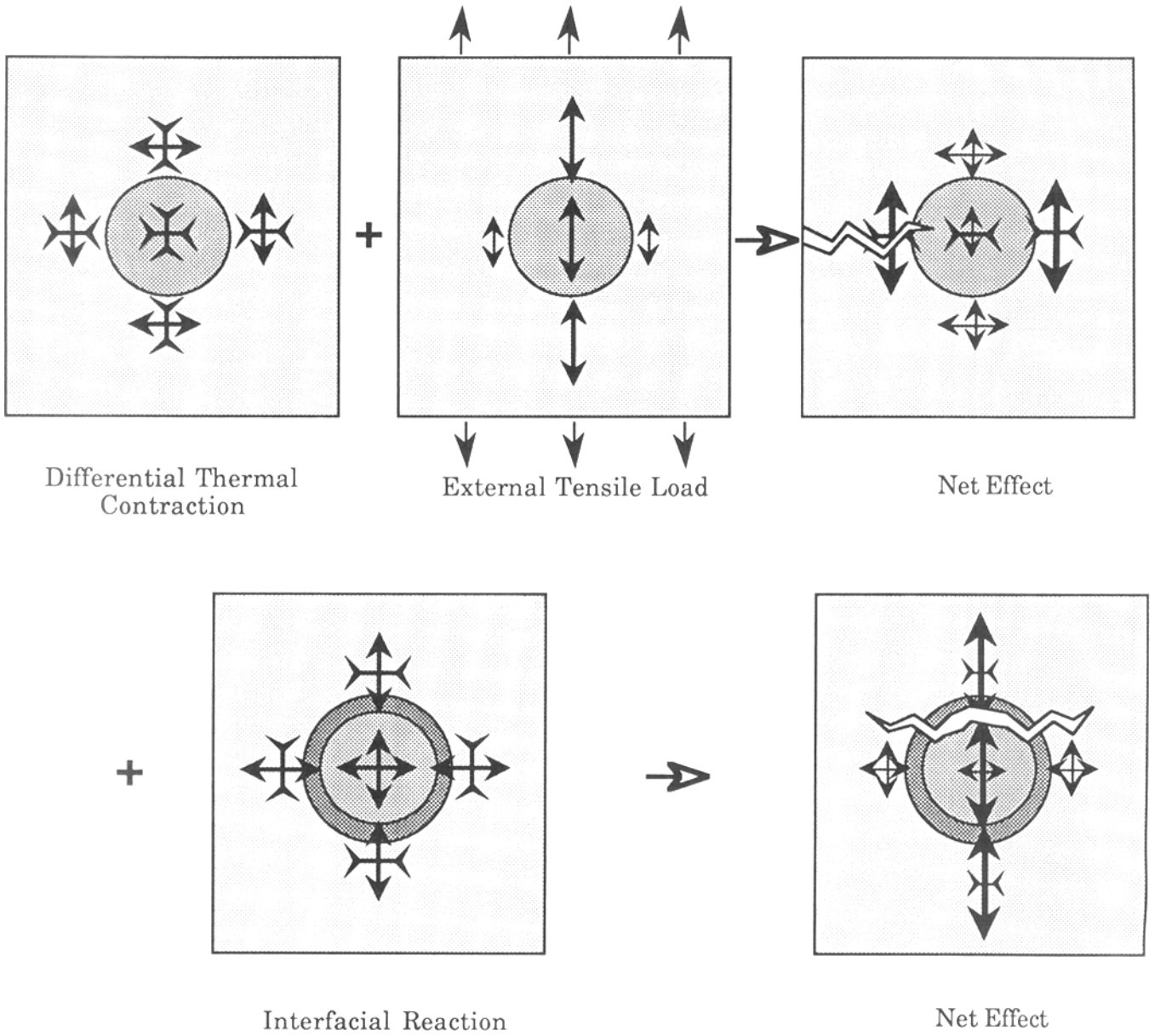

Fig. 11—Schematic illustration of the stress distributions around a SiC particle in a Ti matrix under external load, with and without the effect of a transformation strain arising from the interfacial reaction.

4. The work of fracture of these composites falls with increasing reaction layer thickness, becoming small if this is greater than about 1 to 2 μm. This transition is accompanied by a distinct change in the preferred crack pattern, from one in which the bond strength is high and particle fracture common, to one in which cracking occurs readily at the boundary between the SiC particle and the adjacent reaction layer.
5. The observed changes in fracture behavior have been attributed to changes in interfacial bond strength and also to changes in stress state around the SiC particles, arising from the volume change accompanying the reaction. The transformation involves a linear strain of about −1.5 pct, which probably makes a significant contribution to the radial tensile stress across the interface, even for relatively thin reaction layers. This may be partly responsible for the highly deleterious effects observed to result from interfacial reaction in this system.

ACKNOWLEDGMENTS

Financial support for one of us (AJR) is being provided by Pechiney. The work is integrated with a research program on Ti composites supported by SERC and Ministry of Defence. Useful discussions have taken place with Dr. P. Jarry and Dr. G. Regazzoni of the Pechiney Research Centre at Voreppe. The authors are grateful to Miss A.F. Whitehouse of Cambridge University for carrying out some of the specimen preparation and testing, to Mr. B. Bes for his expertise during the Auger

investigations at Pechiney, to Mr. A. Forno of NPL, Middlesex, for valuable help with the extrusion, and to Mr. K.A. Roberts for his expertise in running the VPS facility at Cambridge.

REFERENCES

1. P. Martineau, M. Lahaye, R. Pailler, R. Naslain, M. Couzi, and F. Cruege: *J. Mater. Sci.*, 1984, vol. 19, pp. 2749-70.
2. C.W. Andersson and R. Warren: *Composites*, 1984, vol. 15, pp. 820-24.
3. C.G. Rhodes and R.A. Spurling: in *Recent Advances in Composites in the United States and Japan*, ASTM STP 684, J.R. Vison and M. Taya, eds., ASTM, Philadelphia, PA, 1985, pp. 585-99.
4. W.J. Wheatley and F.W. Wawner: *J. Mater. Sci. Lett.*, 1985, vol. 4, pp. 173-75.
5. S.K. Choi, M. Chandrasekaran, and M.J. Brabers: *J. Mater. Sci.*, 1990, vol. 25, pp. 1957-64.
6. F.E. Wawner and S.R. Nutt: *Ceram. Eng. Sci. Proc.*, 1980, vol. 1, pp. 709-19.
7. R.L. Mehan, M.R. Jackson, and M.D. McConnel: *J. Mater. Sci.*, 1983, vol. 18, pp. 3195-3205.
8. R.R. Kieschke, R.E. Somekh, and T.W. Clyne: *Proc. ECCM3*, A.R. Bunsell, P. Lamicq, and A. Massiah, eds., Societe Francais de Metallurgie, Bordeaux, France, March 20–23, 1989, pp. 265-72.
9. M. Nathan and J.S. Ahearn: *Mater. Sci. Eng.*, 1990, vol. A126, pp. 225-30.
10. A.G. Metcalfe and M.J. Klein: in *Interfaces in Metallic Matrix Composites, Composite Materials, Vol. 1*, K.G. Krieder, ed., Academic Press, New York, NY, 1974, pp. 310-30.
11. C. Jones, C.J. Kiely, and S.S. Wang: *J. Mater. Res.*, 1989, vol. 4, pp. 327-35.
12. C. Jones, C.J. Kiely, and S.S. Wang: *J. Mater. Res.*, 1990, vol. 5, pp. 1435-42.
13. W. Wei: in *Fundamental Relationships between Microstructure and Mechanical Properties of Metal Matrix Composites*, M.N. Gungor and P.K. Liaw, eds., TMS, Warrendale, PA, 1990, pp. 353-70.
14. M.J. Hartley: *Effect of Isothermal Exposure on the Mechanical Properties of a Continuously Reinforced Fibre Reinforced Titanium Matrix Composite*, in *Proc. 9th Risø Int. Symp. on Mechanical and Physical Behaviour of Metallic and Ceramic Composites*, S.I. Andersen, H. Lilholt, and O.B. Pedersen, eds., Risø National Laboratory, Risø, Denmark, 1988, pp. 383-90.
15. M.H. Loretto and D.G. Konitzer: *Metall. Trans. A*, 1990, vol. 21A, pp. 1579-87.
16. P.A. Dearnley, K.A. Roberts, and T.W. Clyne: *12th Int. Plansee Seminar*, Reutte, Austria, May 1989, H. Bildstein and H.M. Ortner, eds., Deutche Gesellshaft fur Metallkunde, 1989, vol. 3, pp. 523-38.
17. E. Lugscheider: *The Family of Plasma Spray Processes—Present Status and Future Prospects, 1st Plasma Technik Symp.*, Lucerne, Switzerland, May 1988, H.E. Schnauer, P. Huber, A.R. Nicoll, and S. Sandmeier, eds., Plasma Technik, Wohlen, Switzerland, 1988, pp. 23-48.
18. A.R. Stetson and C.A. Hauck: *J. Met.*, 1961, vol. 13, pp. 479-82.
19. H. Gruner, A.R. Nicholl, and D. Prince: in *UK Corrosion 1984*, Institute of Corrosion Science and Technology, London, 1984.
20. R.R. Keischke and T.W. Clyne: *Plasma Processing of Ti-based Composites*, in *Proc. 6th World Conf. on Titanium*, P. Lacombe, R. Tricot, and G. Beranger, eds., Société Franç. de Metallurgie, 1989, pp. 1789-94.
21. A. Daimaru, T. Hata, and M. Taya: in *Recent Advances in Composites in the United States and Japan*, ASTM STP 684, J.R. Vison and M. Taya, eds., ASTM, Philadelphia, PA, 1985, pp. 505-21.
22. D. Apelian, M. Paliwal, R.W. Smith, and W.F. Schilling: *Int. Met. Rev.*, 1983, vol. 28, pp. 271-394.
23. D.G. Konitzer and M.H. Loretto: *Acta Metall.*, 1989, vol. 37, pp. 397-406.
24. *Smithell's Metals Reference Book*, E.A. Brandes, ed., Butterworth's, London, 1983, ch. 14.